Effects of Welding on the Tensile Performance of High Strength Steel T-stub Joints

Cheng Chen [a], Xingzhao Zhang [a], Mingshan Zhao [a,*], Chi-King Lee [c], Tat-Ching Fung [a], Sing-Ping Chiew [b]

[a] School of Civil and Environmental Engineering, Nanyang Technological University, Singapore
[b] Singapore Institute of Technology, Singapore
[c] School of Engineering and Information Technology, University of New South Wales Canberra, Australia

ARTICLE INFO

ABSTRACT

In this study, the effects of welding on the tensile performance of the Reheated, Quenched and Tempered (RQT) S690 high strength steel T-stub joints are investigated by both experimental and numerical methods. Firstly, six RQT-S690 T-stub joints as well as two Thermal-Mechanical Controlled Processed (TMCP) S385 T-stub joints are fabricated and tested. The results are validated against the design plastic resistance equations provided by EC3. It is found out that EC3 predicts the plastic resistance of the TMCP joints conservatively, but tends to overestimate that of the RQT-S690 joints although the latter is much superior. It is deducted that the problem may come from the compromised properties of the heat affected zone (HAZ) at the weld toe. Further, finite element analysis is carried out to investigate the effects of property alteration in the HAZ on the tensile performance of the RQT-S690 T-stub joints. It is shown that the models with welding simulation agree well with the test results, while the models without considering the welding effects predict the load carrying capacity unconservatively when the displacement increases.

© 2016 Institution of Structural Engineers. Published by Elsevier Ltd. All rights reserved.

1. Introduction

Structural steel is one of the most popular materials employed in civil engineering construction due to its high strength, stiffness, toughness and ductile properties [1]. With the development of design, fabrication and technology, the evolution of steels for construction never stops. In the 1900s, most primary structural steel only had nominal yield strengths of about 220 MPa, which is equivalent to today's "mild steel" [2]. The once so called "high strength" steel S355 is now a widely used structural material. In fact, steels with yield strength up to 460 MPa have been commonly specified for applications in many structural design codes [3,4]. What is more, the interest for using high strength (HSS) with minimum yield strength >460 MPa in application have been increasing in the last decade.

Strength of steel is usually enhanced by either adding alloying elements or going through heat treatments/work hardening. Different from high alloy steels, heat treated steels offer better performance in yield and tensile strength without sacrificing much weldability, e.g., low alloy quenched and tempered HSS in grade S690. For many types of HSS such as the quenched and tempered S690 steel, the actual yield strength can be easily double that of grade S355 normal strength steel (NSS). However, HSS differs from NSS in much more aspects than just strength. One major issue against the popularization of HSS is that the quenching and tempering process improves the strength at the expense of ductility through complicated heat treatments. Massive researches have demonstrated that it is not possible for QT steels to achieve good deformation capacity [2,5,6] and they are more susceptible to heat [7, 8] than mild steels, as inherited from the heat-treatment hardened microstructures [9]. Accordingly, it is not surprising that concerns are raised about the performance of welded high performance steel connections, especially when large heat input welding is applied [10]. For conventional steels, it is suggested that if the width of the soft zone does not exceed 25% of the plate thickness, the local softening would not necessarily impair the global strength due to the constraints of the stronger weld metal and unaffected base metal [11,12]. However, this criterion may not apply on high performance steels, because their main constitutes in the microstructures, such as martensite and bainite, are not stable at high temperatures [13]. There is a possibility that the enhanced mechanical properties acquired by means of hardening may deteriorate significantly after exposure to heat, due to microstructural changes at certain critical temperatures [9,14].

The objective of this paper is to investigate the effect of welding on the tensile performance of high strength steel, i.e. Reheated, Quenched and Tempered (RQT) Steel in grade S690 by both experimental and numerical methods. As control material, the Thermal-Mechanical Controlled Processed (TMCP) steel in grade S385 is employed in the experimental program. Eight T-stub joints in the same configuration but different materials and thicknesses are fabricated and tested. Based on the test results in terms of load-displacement curves, the

* Corresponding author.
  E-mail addresses: cchen013@ntu.edu.sg (C. Chen), N1609476D@ntu.edu.sg (X. Zhang), mszhao@ntu.edu.sg (M. Zhao), c.lee@adfa.edu.au (C.-K. Lee), CTCFUNG@ntu.edu.sg (T.-C. Fung), SingPing.Chiew@SingaporeTech.edu.sg (S.-P. Chiew).

first yield resistance is obtained and compared with predictions by design equations provided by EN 1993-1-8 [15]. Further, finite element simulation is carried out to investigate the influence of welding induced HAZ on the tensile performance of the RQT-S690 joints. By comparing the load-displacement curves and the first yield resistance, the effects of welding on the high strength steel T-stub joints are evaluated.

2. Experimental study

2.1. Materials

The RQT is essentially a refined quenching and tempering technology. Compared with traditional directly quenched and tempered steel plates, RQT steel plates exhibit better homogeneity in through-thickness mechanical properties. The RQT grade S690 steel (RQT-S690, 8 mm, 12 mm and 16 mm thick) studied in this paper have a nominal yield strength of 690 MPa, a tensile strength from 790 MPa to 930 MPa and an elongation capacity about 15%. Besides the RQT-S690 as the main research target, another NSS in grade S385 (16 mm thick) is also tested with the same test program as the control material. This NSS is a type of advanced low alloy structural steel plate product manufactured by the Thermal-Mechanical Controlled Process (TMCP). The concept of TMCP combines controlled hot rolling with accelerated cooling to control the microstructure [16]. The goal of TMCP is to produce cost-efficient steel strips and plates with properties required for a specific application. In addition to strength, hardness and toughness, weldability and corrosion resistance are usually made features of TMCP. The TMCP-S385 tested in this study has minimum yield strength of 385 MPa and tensile strength between 550 MPa and 670 MPa.

The stress-strain curves and the summarized mechanical properties of the steel plates obtained by standard coupon tensile test are shown in Fig. 1 and Table 1, respectively. Table 1 also compares the materials properties of the TMCP and RQT plates with the corresponding standards of EN 10025-4 [17] and EN 10025-6 [18], respectively. From Table 1, two distinct features of RQT-S690 steel can be seen. First, this material has superior strengths compared to traditional steels. The actual yield strength of RQT-S690 is twice the nominal yield strength of S355, which is widely used in construction. Second, RQT-S690 steel is relatively brittle compared to traditional NSS and the TMCP-S385 tested in this study. It can also be seen from Table 1 that the TMCP-S385 steel literally fulfilled the mechanical property specifications of S420 M/ML steel.

2.2. T-stub joint specimen fabrication

Four types of T-stub joints were fabricated. They were of the same configuration but fabricated by using different materials and plate thickness: RQT-S690 (8 mm, 12 mm and 16 mm) and TMCP-S385
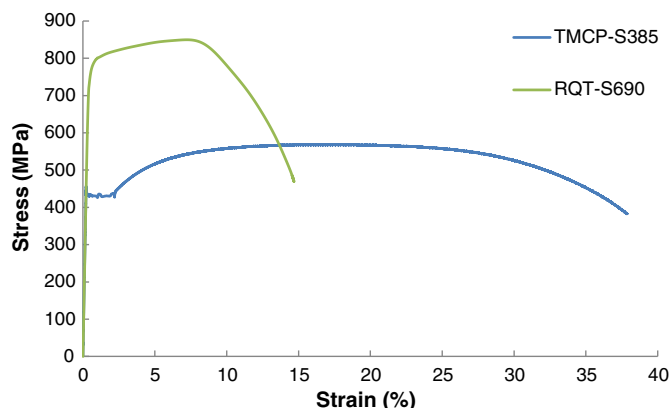

Fig. 1. Stress-strain curves of RQT-S690 and TMCP-S385.

Table 1
Mechanical properties of the TMCP-S385 and RQT-S690 plates tested.

	f_y(MPa)	f_u(MPa)	E (GPa)	Elongation (%)
RQT-S690 (16 mm)	745.2.0	837.8	208.9	14.5
EN 10025-6 S690Q/QL (3 mm ≤ t ≤ 50 mm)	690	770–940	–	14
TMCP-S385 (16 mm)	443.3	568.0	208.4	37.8
EN 10025-4 S420M/ML(t ≤ 16 mm)	420	520–680	–	19

(16 mm). For each type of T-stub joint, two same specimens were fabricated and tested so a total of eight tests were conducted. Each specimen is fabricated by joining two identical steel plates with dimensions of $440 \times 150 \times t$ mm, where t is the thickness of the plates. The joints are designed as *complete penetration butt weld joint* according to the AWS structural steel welding code [19]. Three bolt holes were drilled at each side of the chord plate in order to fix the specimens to the test rig. The distance between two rows of bolt holes (center to center) is 290 mm. The configuration of the joints is shown in Fig. 2 and Shielded Metal Arc Welding (SMAW) was employed to finish the welding connection. Compared to the other common welding methods, SMAW is more "friendly" to martensite-based HSS like RQT S690 steel due to its low heat input [20] which produce less effect on the heat affected zone (HAZ).

2.3. Test set-up and testing procedure

Tensile tests for the T-stub joints were carried out in a servo-hydraulic universal test machine that has a maximum loading capacity of 2000 kN. To fix the specimen into the test machine, "inverted" support joints made of S355 steel plates with thickness of 50 mm were fabricated. The configurations of the support joints are the same as those of the test joints (Fig. 2). The specimens are fixed into the support joints by six M24 high strength hexagon bolts of grade 10.9HR. The full testing setup is shown in Fig. 3. It should be noted that in certain situations, the response of T-stub joints is influenced by the type of bolt assembly. The rational selection of the most suitable bolt type according to the specific structural usage may avoid premature reduction of joint strength for higher levels of joint rotation and provide further rotational capacity [21]. In this study, the consideration in the selection of bolt is to guarantee the bolts work elastically and cause little influence to the load-displacement relationship. This assumption was verified during testing since no obvious plastic deformation was caused to the bolts after unloading.

To capture the load-displacement relationship of the specimens precisely, LVDT was employed to record the real-time displacement at the brace end. Since it would be easier to control the testing time, displacement control instead of force control was used during the testing. The loading rate was set as 1 mm/min for all time so that quasi-static response could be obtained.

2.4. Test results

2.4.1. General descriptions

Fig. 4 presents the test results in terms of the load-displacement curves of the RQT-S690 (8 mm, 12 mm and 16 mm) T-stub joints, while the test results of the TMCP-S385 (16 mm) joint are shown in Fig. 5 in comparison with those of the RQT-S690 (16 mm). Despite that the specimens may fail in different modes at different loadings, these curves are of the same pattern. In general, three stages in the load-displacement curves can be distinguished: (1) the elastic stage, (2) plastic hinge stage and (3) the failure stage, as shown in Fig. 6. In the elastic stage, the stiffness and the elastic modulus govern the behaviors of the joints until yielding takes place. Within this stage, the load increases rapidly with a high load/displacement ratio, which depends on
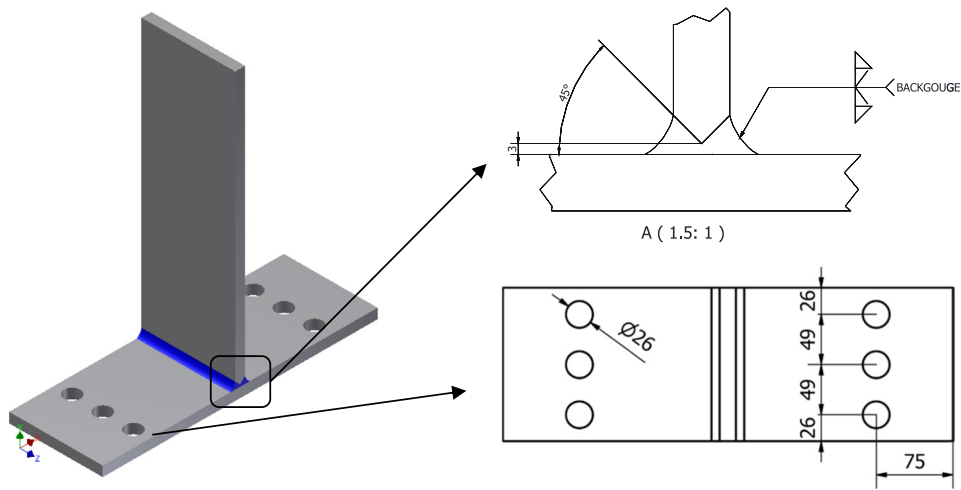
Fig. 2. Configuration of the T-stub joints.

the stiffness of the joint that in turn depends on the material and configuration. When the specimens are further loaded, plastic deformation appears and four obvious plastic hinges could be seen, as shown in Fig. 7. Two of the plastic hinges would appear near the weld toe, and the other two would be near the bolted area. In this stage, the deformation grows more rapidly but the resistance of the joint increases slowly. In general, it is found that the load-displacement curves (Figs. 4 or 5) are generally parallel to each other in this stage. If the loads are further increased, the behavior enters the large deformation stage (failure stage). In this stage, the original configuration of the joint is changed from T to Y shape and the catenary action shows strong existence. The performance of this stage is governed by both the plastic hinge and catenary mechanisms. These two mechanisms further change the stress regime from flexural forces only to combined flexural and axial forces. Compared to the increased plastic hinge moment resistance due to strain hardening, the catenary forces contribute more to the total load carrying capacity. As a result, the strain concentration in the plastic zone and welds is also affected. Due to the lack of sufficient ductility that is required to support the development of plastic hinge and catenary mechanisms, the final failure modes usually happen in the form of weld toe through thickness fracture or bolt hole necking failure (net section failure under tension).

2.4.2. Stiffness and first yield resistance

For design purpose, the behavior of the joints under the elastic stage and the first yield resistance (design plastic resistance) is of the most importance. From Figs. 4 and 5, it can be seen that not only the stiffness but also the deformation limit of the elastic stage varied according to the thickness and steel grade of the specimens. To quantitatively evaluate the effects of these two parameters, the elastic stage and plastic hinge stage of the curves are taken out and simplified into a straight line model (Fig. 8). The intersection of the two straight lines or the turning point of the model is defined as the first yield resistance of the joint, which is widely accepted as the design plastic resistance of the joint before large deformation appears [5,15]. Based on this simplified load-displacement model, the global stiffness of the studied T-stub joints under the elastic stages is defined as:

$$E_G = \frac{F_L}{d} \tag{1}$$

where E_G is the global stiffness and F_L is the applied load (or resistance) at a certain level of elastic displacement d.

The stiffness based on the test results for all the tested joints are listed in Table 2. It can be seen from Table 2 that the difference between the 2 tests of the same type are negligible, implying that the test results are consistent and repeatable. The maximum differences between specimens occurred for the 8 mm and 16 mm RQT-S690 specimens are only 3.2% (row 4, Table 2). Table 2 also shows that the stiffness in terms of applied load (kN) per displacement (mm) increased rapidly with the thickness of the specimens. The stiffness of the 16 mm RQT specimens
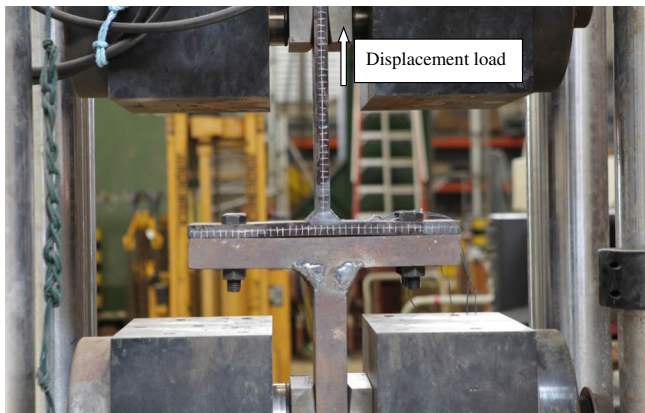

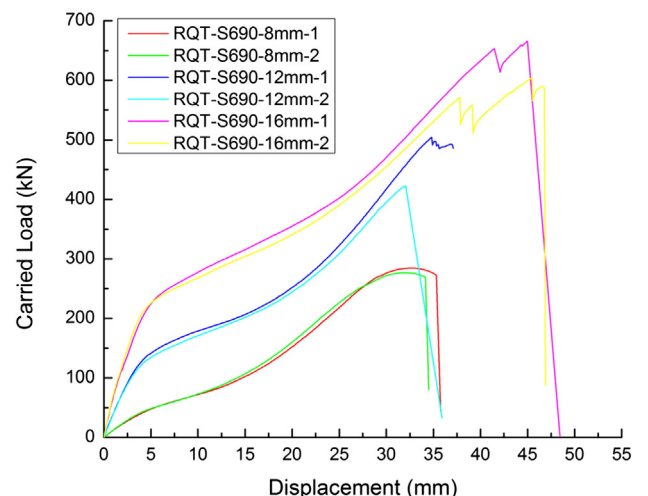**Fig. 3.** The T-stub joint test setup.

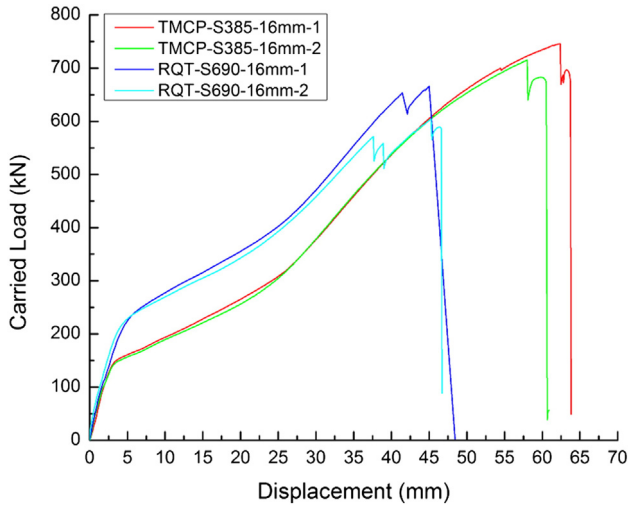**Fig. 4.** Load-displacement curves of the RQT-S690 T-stub joints.

Fig. 5. Load-displacement curves of the TMCP-S385 T-stub joints in comparison with RQT-S690 (16 mm).

(column 4, Table 2) is about 5.3 times of that of the 8 mm RQT specimens (column 2, Table 2) and 1.66 times of that of the 12 mm RQT specimens. In addition, despite that the 16 mm RQT-S690 specimens and the 16 mm TMCP-S385 specimens had the same thickness, the 16 mm RQT-S690 specimens showed slightly higher stiffness (columns 4 and 5, Table 2).

In EC3, to estimate the design resistance of T-stub joints, three failure modes, namely (1) complete yielding of the flange, (2) bolt failure with yielding of the flange and (3) bolt failure [15] are identified. In this study, all the specimens were failed by complete yielding of flange. To predict the design resistance of a T-stub joint when it is failed in complete yielding of the flange, two methods based on the yield line analysis are adopted, as specified by EC3 [15].

$$\text{Method 1}: F = \frac{4M_{pl,1,Rd}}{m} \tag{2}$$

$$\text{Method 2}: F = \frac{(8n-2e_w)M_{pl,1,Rd}}{2mn-e_w(m+n)} \tag{3}$$

In Eqs. (2) and (3), $M_{pl,1,Rd} = l_{eff}\left(\frac{t}{2}\right)^2 f_y$ is the design moment resistance of the section. l_{eff} is the effective width of the T-stub flange of the joint (Fig. 6.2 of [10], 150 mm in this study), m, n are geometrical parameters of the T-stub joints (Fig. 10). e_w is either equal to 1/4 of the washer diameter or the width across points of the bolt head of nut, as relevant [10]. Note that in Method 2, instead of concentrated at the center line of the bolt, it is assumed that the force applied to the T-stub flange by a bolt is distributed uniformly under the washer (or the bolt
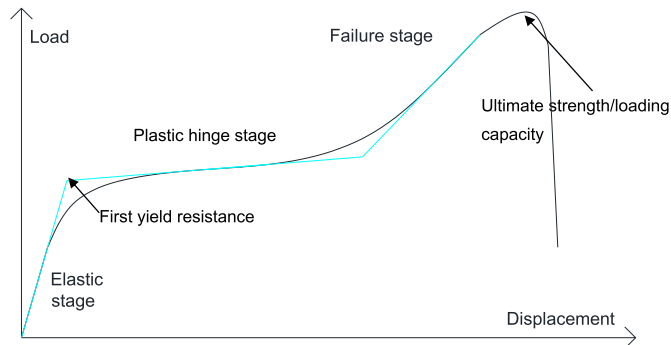

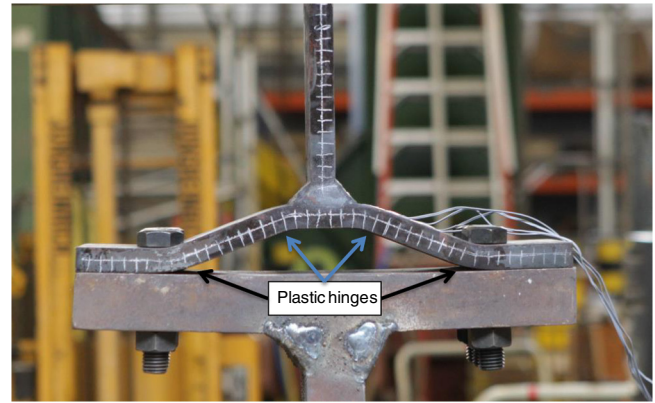Fig. 6. Typical load-displacement curve of T-stub joints.
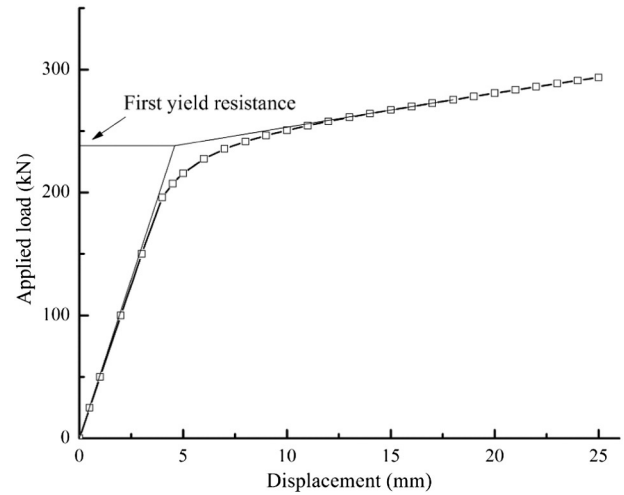

Fig. 7. Plastic hinges formation.

Fig. 8. Simplified elastic-plastic load-displacement curve and design plastic resistance of T-stub joint.

head/nut). Since the distance between the center lines of the weld toe plastic hinge and the bolt area plastic hinge is smaller than m (especially at the beginning of the plastic hinge development stage), this assumption leads to higher but more realistic resistance.

The design resistance of the studied T-stub joints obtained by Eqs. (2) and (3) and the actual resistance obtained from tests are shown in Table 3 and plotted in Fig. 10. Table 3 and Fig. 10 show that the design resistances of the RQT specimens are superior when compared with the TMCP specimens. The average design resistance of 16 mm RQT-S690 specimens is about 91.3% more than that of 16 mm TMCP-S385 specimens. However, the test results of the RQT-S690 specimens are all lower than that predicted by the EC3 equations. The actual first yield resistances of 8 mm RQT-S690 specimen when yielding occurred are lower than Eqs. (2) and (3) by 19.4% and 24.6%, respectively; those of the 12 mm and 16 RQT-S690 specimens are generally lower than Eqs. (2) and (3) by 4% and 10%, respectively. On the other hand,

Table 2
Stiffness of the joint at the elastic stage.

	RQT-S690			TMCP-S385
Thickness (mm)	8	12	16	16
Stiffness (kN/mm) Test1	11.5	37.7	61.0	59.3
Stiffness (kN/mm) Test2	11.8	37.2	63.0	58.1
Diff 1(%)	3.2	−1.5	3.2	−2.0
Average	11.6	37.4	62.0	58.7

Diff 1(%) = (Test2 − Test1) / (Test1) × 100%.

Table 3
Design plastic resistance of the studied T-stub joints.

Thickness (mm)		Test Results (kN)			EC3 Eqs. (kN)		Diff 1(%)	Diff 2 (%)
		Test1	Test2	Average	Eq. (2)	Eq. (3)		
RQT-S690	8	44.2	41.9	43.1	53.4	57.1	− 19.4	− 24.6
	12	126.3	118.4	122.4	123.8	132.7	− 2.4	− 8.9
	16	217.8	219.5	218.7	227.1	243.6	− 3.7	− 10.2
TMCP-S385	16	146.5	142.0	144.3	135.1	144.9	6.8	− 0.4

For Eqs. (2) and (3), the actual yield strengths are used. That is, $f_y = 745.2$ and 443.3 MPa for RQT-S690 and TMCP-S385, respectively.
Diff 1 = ((Average − Eq. (2)) / Eq. (2)) × 100%.
Diff 2 = ((Average − Eq. (3)) / Eq. (3)) × 100%.

the test results of the TMCP specimens are well predicted by Eqs. (2) and (3): only 6.8% higher than Eq. (2) and 0.4% lower than Eq. (3). Based on these test results, it appears that the EC3 equations are conservative when predicting the design resistance for the TMCP-S385 joints but not for the RQT-S690 joints.

Despite that the RQT-S690 steel has shown superior behaviors during the elastic and the plastic hinge stages when compared with the TMCP-S385 steel, the deformation capacities and the ultimate loading capacities of the RQT-S690 specimens are worse than the TMCP specimens. As shown in Fig. 5, the load-displacement curves of these two series of specimens are very similar. They showed almost the same stiffness, similar plastic hinge and failure stages. The major differences are that both the ductility (in terms of ultimate displacement) and the ultimate load carrying capacities of the 16 mm RQT-S690 joints are *worse* than the 16 mm TMCP-S385 joints. Due to the higher ductility of the materials and the deformation capacity of TMCP plates, the 16 mm TMCP-S385 specimens absorbed more strain energy and sustained larger deformation (which helped to increase the ultimate load carrying capacity by changing the shape of the joint from T to Y) before failure than the 16 mm RQT-S690 joints. This also indicated that T-stub joints fabricated by using RQT-S690 steel may not be good for applications such as earthquake resistance structures which demand high ductility and energy dissipation/absorption capacity.

3. Finite element analysis

3.1. Finite element model

According to the recent material property study of HSS RQT-S690 conducted by Chiew et al. [22], the mechanical properties of the RQS-S690 HSS will be affected and deteriorated after exposure to high temperatures. Since welding always induces localized, large and transient heat input into the fusion zone and HAZ, the mechanical properties of HSS will be affected and changed there. Thus, the moment resistance of the plastic hinge at the weld toe may be altered by welding and different from (less than) that at the bolt area. As a result, the moment

resistance at the weld toe can no longer be predicted accurately by the yield line method. However, as both the heat inputs and the size of the HAZ will be decreased when the thickness of the plate is decreased, the impact of such welding effects on the accuracy of the yield line method will also be decreased. This explains why the differences between the plastic resistances predicted by the yield line method and the test results for the RQT-S690 8 mm joints were much smaller than that for the 16 mm joints. In order to verity this deduction, finite element analysis is carried out by using commercial software ABAQUS to investigate the effect of welding heat input on the performance of HSS T-stub joints at elastic and plastic hinge stages.

Two models are built for each of the 8 mm, 12 mm and 16 mm RQT-S690 T-stub joint with exact the same geometrical dimensions as the test set-up (T-stub specimen, the reverse T support and the bolts, as shown in Fig. 3). One model include the mechanical property alteration caused by welding heat input, while the other is an ideal model without simulating the welding process. The experimental study shows that although the tested T-stub specimens were made of different materials or had different thicknesses, the four plastic hinges (Fig. 7) are always critical in determining both the load carrying capacity and final failure mode. Therefore, efforts are made to increase the mesh density at the welded joint zone (zone J) and the bolt-hole zone (zone B), as shown in Fig. 11. As can been seen from Fig. 11, the mesh in zone J is further divided into 5 sub-zones from J-1 to J-5: J-1 is the base metal of the brace; J-3 is the fusion zone during welding and the molten base metal is not considered in this model; J-2 and J-4 is the welding affected zones adjacent to J-3; and J-5 is the base metal of the chord. The concept of this mesh dividing topology is to decompose the whole problem domain into simpler and less problem-affected zones, and therefore improve the modelling efficiency and flexibility in generating meshes for different specimens.

3.2. Solution strategy

The modelling is based on a sequentially coupled thermal-stress analysis, assuming that the changes in stress/displacement depend on the temperature field variation but there is no inverse dependency between the two. Firstly, the pure heat transfer in welding is solved in a transient thermal analysis to obtain the time-dependent temperature distribution fields. Secondly, the time-dependent temperature distribution data is output as thermal loading to the mechanical analysis to simulate the alteration in the mechanical properties and subsequent tensile test.

"Hard" contact is defined for normal behavior of contacts among T-stub, bolts and supporter. In view of the complexity of tangential behavior in contacts (e.g., rough surfaces and pre-tension force in bolts), a simplified contact is adopted. Penalty friction is defined as the tangential behavior of contacts with a friction coefficient 0.3, and the pre-tension forces in bolts are ignored. Thermal and physical boundary
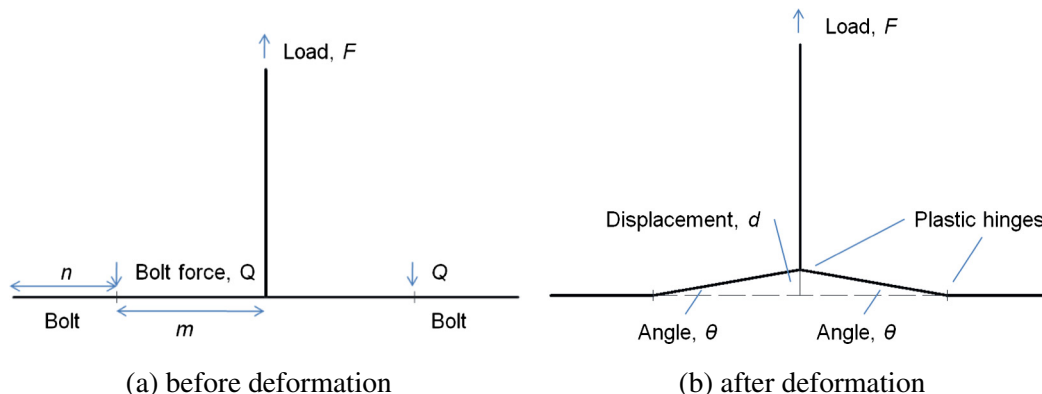

(a) before deformation   (b) after deformation

Fig. 9. Force diagram for design plastic resistance calculation.
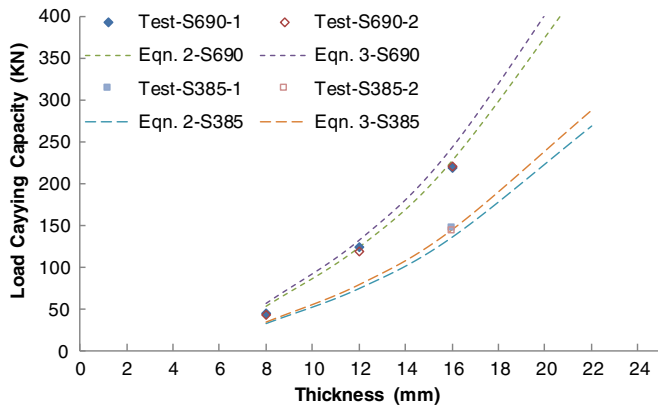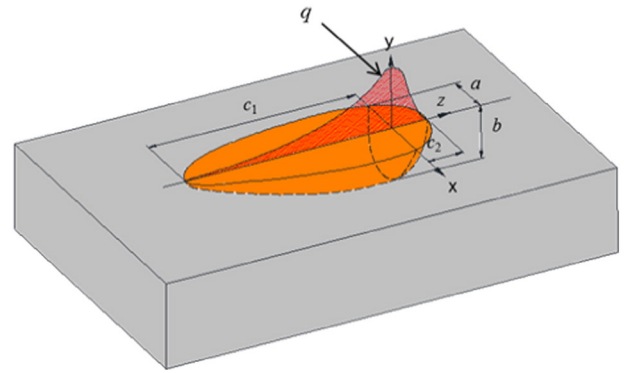
Fig. 10. Design plastic resistance of tested joints.

conditions are defined in thermal and stress analysis models separately. The room temperature is assigned as 25 °C. Convection and radiation boundary assigned on the surfaces of T-stub with the coefficients 25 W/(m^2·°C) and 0.3, respectively.

3.2.1. Heat source

There are two common methods used to simulate the moving heat source in welding: the surface heat and body heat models. Both methods can work with or without element birth and death techniques to simulate the adding of weld fillers. The surface heat model inject heat only on the surface that is close to the interested area, while the body heat model simulated the full impact of welding on the adjacent materials. Jin et al. [23] studied the accuracy and efficiency of both methods on the RQT-S690 plate-to-plate T/Y joints and found out that the body heat source model base on Goldak's double ellipsoid heat source model theory [24] produced the best results.

In this study, the double-ellipsoid heat source is also adopted in the thermal analysis by using the subroutine DFLUX [25], as shown in Fig. 12. Each welding profile is finished by 6 welding passes.

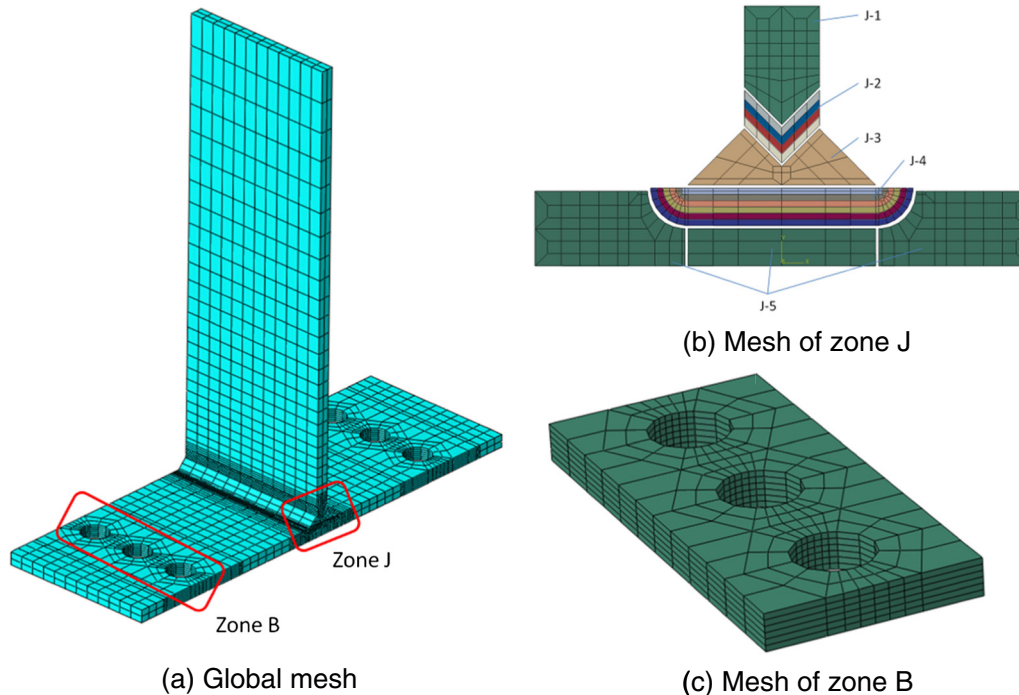The heat flux q is represented by the following equations:

Fig. 12. Double-ellipsoid heat source.
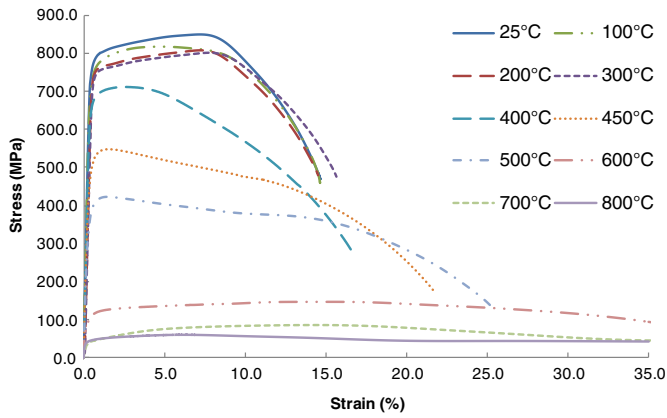
For the front part of heat source

$$q(x,y,z,t) = \frac{6\sqrt{3}Qf_1}{abc_1\pi\sqrt{\pi}}e^{-\frac{3x^2}{a^2}-\frac{3y^2}{b^2}-\frac{3z^2}{c_1^2}} \quad (4)$$

For the rear part of heat source

$$q(x,y,z,t) = \frac{6\sqrt{3}Qf_2}{abc_2\pi\sqrt{\pi}}e^{-\frac{3x^2}{a^2}-\frac{3y^2}{b^2}-\frac{3z^2}{c_2^2}} \quad (5)$$

In Eqs. (4) and (5), f_1 and f_2 are heat distribution coefficients. It is assumed that f_1 is the same as f_2, and equals to 1.0. The parameters a, b, c_1 and c_2 represent the dimensions of molten pool, which are 8.0 mm, 17.0 mm, 8.0 mm and 16.0 mm, respectively. The heat input power Q ($Q = UI$) is equal to 2.56 kJ/mm. In view of the energy dissipation during welding, the energy efficiency coefficient is assumed to be 0.8. Additionally, welding speed is 4 mm/s, and there is no interruption between the two pass welding.

3.2.2. Thermal properties

In this modelling, the involved material-related characteristics include thermal conductivity, specific heat, thermal expansivity, elastic

(b) Mesh of zone J

(a) Global mesh

(c) Mesh of zone B

Fig. 11. Mesh of the T-stub joint.

Fig. 13. Stress-strain curves of S690 HSS at elevated temperatures by [21].

Fig. 15. Temperature distribution during welding of the T-stub joint.

modulus and Poisson's ratio and plasticity [26]. For most steels, many of these physical properties are almost the same, except for the plasticity. Design standards for steel structures under high temperatures such as EN 1993-1-2 [4] provide well defined reduction curves or equations for these properties under elevated temperatures, while the stress-strain relationship of the RQT-S690 HSS under elevated temperatures and after heated and cooled down are obtained from papers written by Chiew et al. [22]. The simplified "heating" and "cooled down" stress-strain curves based on [22] are shown in Figs. 13 and 14, respectively.

3.3. Results and discussion

Fig. 15 shows an example of the temperature distribution during welding the T-stub joint. It can be seen from Fig. 15 that this welding heat input is highly localized around the welding pool and the adjacent materials are fully affected by this heat input.

Fig. 16 shows the T-stub joint at small deformation stage by finite element simulation. It can be seen from Fig. 16 that the deformed shape is the same as the experimental record (Fig. 7). Highly concentrated stresses can be observed at the weld toe and bolt area where the plastic hinges are formed, while the stress level at elsewhere is much lower. Similar to the stress distribution, large deformation can only be found at the plastic hinge areas. As a result, the final failure mode is either weld toe failure or the bolt hole area net cross section failure. It should be noted that the stress level at the bolt hole net cross section is obviously higher than that at the weld toe cross section (Fig. 16) because of the smaller net cross section. However, the weld toe failure mode is
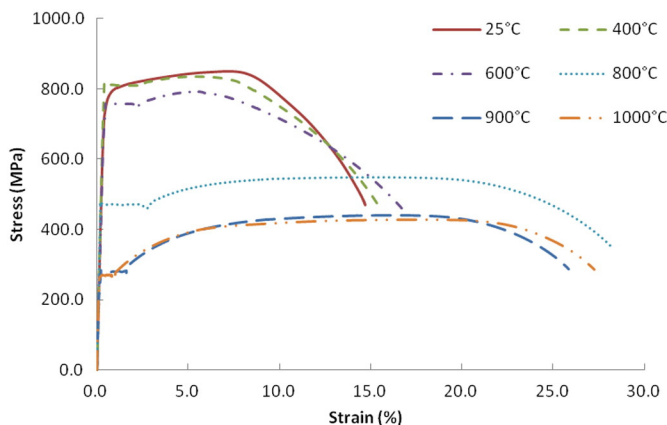
more likely to take place because the load carrying capacity of the HAZ is much lower, as one of the most significantly effect of welding.

Further, the load-displacement (see definition in Figs. 3 and 9) curves of the 8 mm, 12 mm and 16 mm RQT-S690 T-stub joints are output and shown in Figs. 17–19, respectively. It can be seen from Figs. 17–19 that the models with HAZ simulation (FE-w/ HAZ) agree well with the test results. Although these FE-w/ HAZ curves tend to be slightly higher than the test results, the elastic stage is well predicted until plastic hinges are formed. On the other hand, the models without HAZ (FE-w/o HAZ) simulation overestimate the load resistance. Only the elastic stiffness when the models are initially loaded agree with the test curves, while both the elastic stiffness at relatively large deformation and the load resistance is much higher than the test results.

According to the simplified approach for determining the first yield resistance (Fig. 8), the first yield resistance of the FE models is obtained and compared with the test results, as shown in Table 4. It can be seen from Table 4 that the resistance of the FEM-w/o HAZ series is at least 18% higher than that of the Test-Ave, while difference between the FEM-w/ HAZ series and the Test-Ave is generally within 10%. Therefore, it can be concluded that welding has significant impact on the strength of high strength steel RQT-S690 T-stub joints. Without considering this impact would lead to overestimation on the load carrying capacity and may be unsafe in practice.

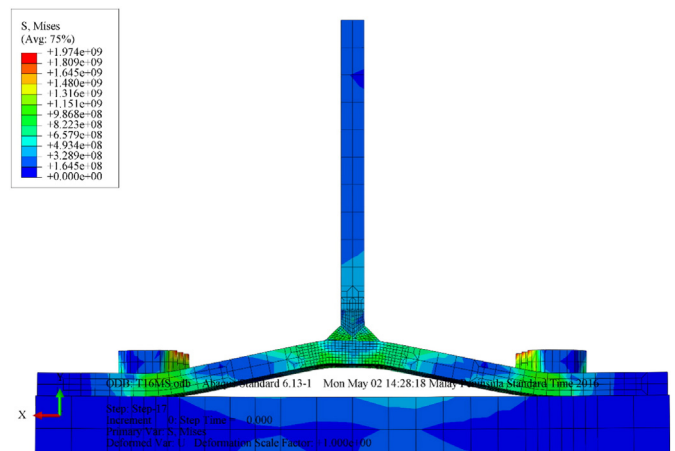Fig. 14. Stress-strain curves of S690 HSS after exposure of certain high temperatures by [21].

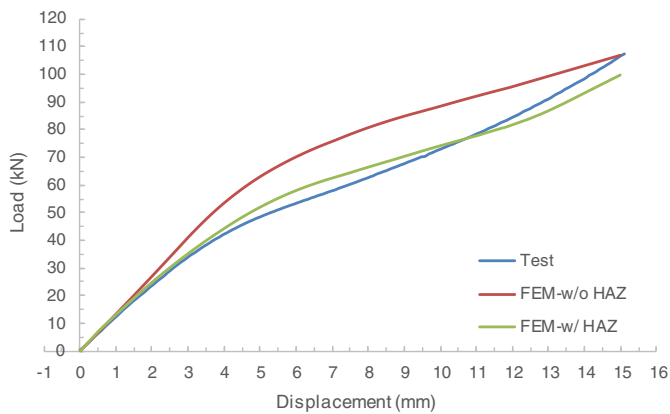Fig. 16. Stress distribution of the T-stub (16 mm) at small deformation stage.

Fig. 17. Load-displacement curves of the 8 mm RQT-S690 T-stub joints.
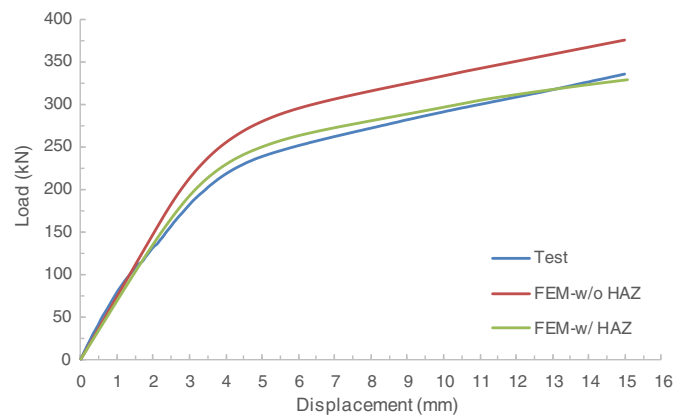

Fig. 19. Load-displacement curves of the 16 mm RQT-S690 T-stub joints.

4. Conclusions

This study investigated the effects of welding on the tensile performance of the Reheated, Quenched and Tempered (RQT) S690 high strength steel T-stub joints in two phases. The first phase experimentally investigates the tensile behavior of six RQT-S690 T-stub joints, and the Thermal-Mechanical Controlled Processed (TMCP) steel in grade S385 is also tested with same program as control material. By comparing the load-displacement curves, it is found that the behavior of these two material is of the same pattern. The EC3 design resistance prediction equations predict the first yield resistance of the TMCP-S385 specimens conservatively, but seem to overestimate that of the RQT-S690 joints. Further discussion deducts that the problem may come from the compromised properties of the plastic hinges at the weld toe, which is highly possible to be affected by welding heat input. Phase II of this study verifies this deduction by finite element analysis. It is shown that models with welding simulation agree well with the test results, while the models without considering the welding effects predict the load carrying capacity unconservatively when the displacement increases. Finally, it is concluded that welding has significant impact on the strength of high strength steel RQT-S690 T-stub joints. Without considering this impact would lead to overestimation on the load carrying capacity and may be unsafe.
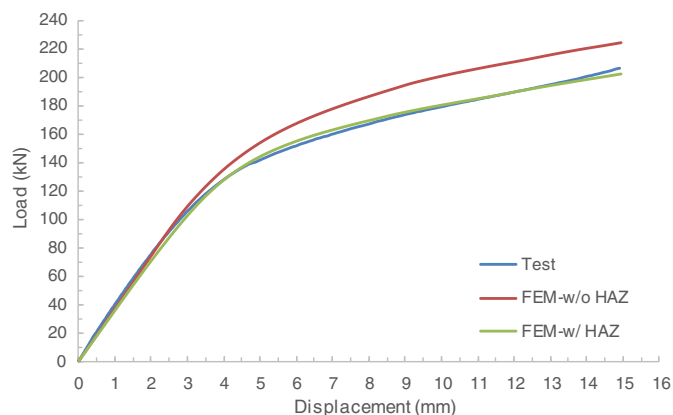
Table 4
First yield resistance of the FE simulation compared with the test results.

Specimen		Test-Ave	FEM-w/o HAZ	Diff 1 (%)	FEM-w/ HAZ	Diff 2 (%)
RQT-S690	8 mm	43.1	53.7	24.6	47.3	9.7
	12 mm	122.4	146.3	19.5	132	7.8
	16 mm	218.7	258.2	18.1	230	5.2

Note: Diff 1 = ((FEM-w/o HAZ − Test-Ave) / Test-Ave) × 100%.
Diff 2 = ((FEM-w/ HAZ − Test-Ave) / Test-Ave) × 100%.

References

[1] Bjorhovde R, Engestrom M, Griffis L, Kloiber L, Malley J. Structural steel selection considerations: Reston (VA) and Chicago (IL): American Society of Civil Engineers (ASCE) and American Institute of Steel Construction (AISC); 2001.
[2] Bjorhovde R. Development and use of high performance steel. J Constr Steel Res 2004;60:393–400.
[3] AISC. Specification for structural steel buildings. ANSI/AISC 306-05, ed. Chicago: Americal Institute of Steel Construction; 2005.
[4] BSI. Eurocode 3: design of steel structures: part 1–1 general rules and rules for buildings, BS EN 1993-1-1, ed. London: British Standard Institution; 2005.
[5] Girão Coelho AM, Bijlaard FSK. Experimental behaviour of high strength steel end-plate connections. J Constr Steel Res 2007;63:1228–40.
[6] Uy B. Stability and ductility of high performance steel sections with concrete infill. J Constr Steel Res 2008;64:748–54.
[7] Chen J, Young B. Behavior of High strength structural steel at elevated temperatures. J Struct Eng 2006:P1948–54.
[8] Qiang X, Bijlaard F, Kolstein H. Dependence of mechanical properties of high strength steel S690 on elevated temperatures. Constr Build Mater 2012;30:73–9.
[9] Bhadeshia HKDH, Honeycombe RWK. Steels: microstructure and properties. 3th ed. Oxford, United Kingdom: Elsevier Science & Technology; 2006.
[10] Zhao MS, Chiew SP, Lee CK. Post weld heat treatment for high strength steel welded connections. J Constr Steel Res 2016;122:167–77.
[11] d. M. B. The weldability of modern structural TMCP steels. ISIJ Int 1997;37:537–51.
[12] Hochhauser F, Ernst W, Rauch R, Vallant R, Enzinger N. Influence of the soft zone on the strength of welded modern HSLA steels. Weld world 2012;56:77–85.
[13] Verhoeven JD. Steel metallurgy for the non-metallurgist. Ohio, USA: ASM International; 2007.
[14] Sverdlin AV, Ness AR. Chapter 3: fundamental concepts in steel heat treatment (steel heat treatment handbook: metallurgy and technology. Taylor & Francis Group; 2007.
[15] BSI. Eurocode 3: design of steel structures: part 1–8 design of joints, BS EN 1993-1-8, ed. London: British Standard Institution; 2005.
[16] Machida S, Kitada H, Yajima H, Kawamura A. Extensive application of TMCP steel plates to ship hulls: 40 kgf/mm2 class high yield stress steel. Mar Struct 1988;1: 219–43.

Fig. 18. Load-displacement curves of the 12 mm RQT-S690 T-stub joints.

[17] BSI. Hot rolled products of structural steels: part 4 technical delivery conditions for thermalmechanical rolled weldable fine grain structural steels, BS EN 10025-4, ed. London: British Standards Institution; 2004.

[18] BSI. Hot rolled products of structural steels: part 6 technical delivery conditions for flat products of high yield strength structural steels in the quenched and tempered condition, BS EN 10025-6, ed. London: British Standards Institution; 2004.

[19] AWS. Structural Welding Code, in steel, ed. Miami: American National Standards Institute; 2008.

[20] Mohandas T, Madhusudan Reddy G, Satish Kumar B. Heat-affected zone softening in high-strength low-alloy steels. J Mater Process Technol 1999;88:284–94.

[21] D'Aniello M, Cassiano D, Landolfo R. Monotonic and cyclic inelastic tensile response of European preloadable GR10.9 bolt assemblies. J Constr Steel Res 2016;124:77–90.

[22] Chiew SP, Zhao MS, Lee CK. Mechanical properties of heat-treated high strength steel under fire/post-fire conditions. J Constr Steel Res 2014;98:12–9.

[23] Jin YF, Zhao MS, Lee CK, Chiew SP. Influence of welding on high strength steel plate-to-plate joints - part I: simulation of residual stress, presented at the 11th international conference on steel. Qindao, China: Space and Composite Structures; 2012.

[24] Goldak J, Chakravarti A, Bibby M. A new finite element model for welding heat source. Metall Trans 1984;15B:299–305.

[25] ABAQUS. ABAQUS Analysis user's manual version 6.9: ABAQUS Inc; 2009.

[26] Bhadeshia HKDH. Material factors (handbook of residual stress and deformation of steel). University of Cambridge; 2002.